Ⓔ

First Steps toward a Reassessment of the Seismic Risk of the City of Dushanbe (Tajikistan)

by Marco Pilz, Dino Bindi, Tobias Boxberger, Farhod Hakimov, Bolot Moldobekov, Shohrukh Murodkulov, Sagynbek Orunbaev, Massimiliano Pittore, Jacek Stankiewicz, Shahid Ullah, Firoz Verjee, Marc Wieland, Pulat Yasunov, and Stefano Parolai

Online Material: Table detailing station installation sites and recording times.

INTRODUCTION

The country of Tajikistan is located in the Asia–India continental collision zone where the northward-moving Indian plate indents the Eurasian plate (Molnar and Tapponnier, 1975). The Asian lithosphere being impinged upon by the shallow northward underthrusting Indian lithosphere has resulted in high-mountain topography, which is subject to active deformation and contemporary faulting, and, consequentially, frequent earthquakes (e.g., Gubin, 1960; Burtman and Molnar, 1993). According to the Global Seismic Hazard Map (Giardini, 1999), almost the entire country exhibits a high-hazard level with intensities of VIII–IX for a 5% exceedance in 50 years. Most of the earthquakes that occur in these fault zones are crustal events with dominating thrust faulting along the Pamir front, whereas on the eastern edge of the Pamir the style of deformation is generally characterized by oblique thrusting with a component of strike-slip motion. Thrust-type events beneath the Tadjik Depression, a compressional intermountain basin in the western part of the country, indicate that both the sedimentary rocks and the basement are involved in shortening (Fan *et al.*, 1994; Delvaux *et al.*, 2013).

Although archaeological remnants dating to the fifth century B.C. have been discovered in this area, there is little to suggest that Dushanbe, the Tajik capital, was more than a small village until the early twentieth century. Therefore, there exists only a relatively short record of strong earthquakes in the area (e.g., the 1907 **M** 7.3 Karatag earthquake and the 1949 **M** 7.4 Khait earthquake) in comparison with other parts of Central Asia. The General Seismic Zoning map for the former Soviet Union (GSZ-78) associated an intensity of IX to Dushanbe, with a recurrence interval of 1000 years (Bune and Gorshkov, 1980). Recently, Nurmangambetov *et al.* (1999) calculated refined return periods for intensities IX and VIII of 1995 and 447 years, respectively. One reason for the high-hazard level is the fact that the town is located close to two main fault systems. The South Gissar fault is located a few kilometers north of the city and the estimated maximum magnitude associated with this fault is 7.5 (Fig. 1). The second is the Ilek–Vaksh fault, about 25 km south of Dushanbe, and is characterized by a maximum magnitude of 6.5 (Babaev *et al.*, 2005).

Given the high seismic hazard in this area, the first seismic zonation for Dushanbe was derived as early as 1937, based on the area's geotechnical and hydrogeological conditions (Tsshoher, 1938), assigning a Mercalli intensity of VIII for the southern and western parts of the city and VII for the northern and eastern parts. In contrast to these earlier findings, opposite variations in macroseismic intensity were observed during the 1949 Khait (modern spelling Hoit) earthquake (**M** 7.4; Rautian and Leith, 2002), which occurred around 250 km northeast of Dushanbe. In the northern and eastern parts of the city ground shaking was felt more strongly and cracks in several hundred buildings were observed, whereas for the southern parts, the level of shaking was lighter (Katok, 1965).

The studies following the 27 February 1952 event (M_s 4.7 $\pm$ 0.2), the epicenter for which was only about 25 km north of the center of the city, mark a milestone. For the first time, detailed macroseismic investigations were carried out (Medvedev, 1952), assigning an Medvedev–Sponheuer–Karnik (MSK) intensity of VI to Varzob, a small village close to the epicenter located on rock, as an intensity of VI–VII has been assigned to the northeastern part of Dushanbe. For the western and southern parts of the city an intensity of only V had been mapped, whereas for Koktash, around 13 km south of the city, the assigned intensity was VI. Correspondingly, also for the Sultanabadskoe earthquake on 7 July 1953 (M_s 4.4 $\pm$ 0.1), the epicenter of which was around 30 km

 doi: 10.1785/0220130040

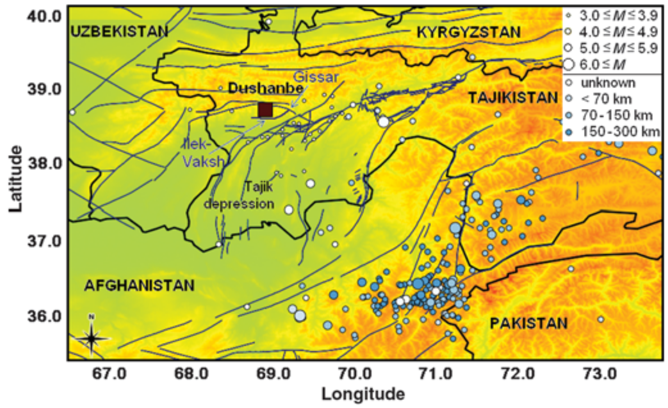

▲ **Figure 1.** Location of Dushanbe. The epicenters of the local and regional earthquakes used in this study (color coded with depth) and the main active faults (blue lines, Trifonov *et al.*, 2002) are indicated. Faults mentioned in the text are labeled.

southeast of the city center, shaking was felt more strongly in the northeastern districts of Dushanbe than in the southern parts. Thereon, mainly based on the first-mentioned event, Nazarov and Nechaev (1953) published a new zonation map for Stalinabad (the former name of Dushanbe) including also strong-motion data. In their map, an intensity of IX was assigned to large areas in the northeast and to the western and northwestern parts of the city, whereas along a stripe in the center and for parts in the southeast the assigned intensity was VIII.

In the 1960s a significant increase in Dushanbe's population and the use of new construction types for buildings made it desirable to establish a new seismic zonation. Because seismic hazard in Dushanbe is related not only to shallow local earthquakes but also to deep-focus distant earthquakes, two different zoning maps were proposed for the town, one for buildings with less than five storeys and another one for taller buildings (Cohen *et al.*, 1975). Later on in the 1990s, minor refinements of these seismic zoning maps for the territory of Dushanbe were carried out, mainly in connection with the new settlements in the western and southwestern parts (Negmatulaev, Ischuk, Potekhin, 1999).

The high level of seismic risk in Tajikistan is not only dictated by the high level of seismic hazard, but it also depends on the vulnerability of the buildings. Conservative estimates assume that 55,000 fatalities and 220,000 serious injuries might result from intensity IX shaking in Dushanbe alone (Khalturin *et al.*, 1997). However, destruction of this magnitude should not be surprising given that the majority of the newly constructed residential buildings in Dushanbe (mainly 1–3 storey brick houses) do not adhere to seismic design standards and are therefore highly vulnerable (Negmatulaev, Ischuk, Potekhin, 1999), whereas its older Soviet-era residential buildings have also been found to perform poorly during earthquakes (e.g., Pomonis, 1990). Moreover, most of buildings on the left bank (i.e., eastern) part of Dushanbe city had been already constructed before the 1960s, the period when calculating seismic standards for designed and constructed buildings in the city was lower in comparison with design seismicity adopted at the present time.

Improvements in our level of knowledge as well as the speed and direction of urban growth in recent years has emphasized the need to update the information on seismic site conditions and building-stock vulnerability for Dushanbe. In particular, during the last two decades, Dushanbe has expanded rapidly beyond the edges of the city, mainly in southern direction along the Varzob river (on geologically unfavorable material, see Geological and Geophysical Setting section), but also up the slopes of the fringing mountain ranges in the northeast. The areas along the mountain slopes are particularly prone to soil liquefaction and show potential for (possibly earthquake-triggered) landslides. Multitemporal change detection using a postclassification comparison method (Wieland *et al.*, 2012a) points out that in 1972 a total area of 54 km^2 was classified as being built up in the greater Dushanbe urban area, whereas in 2010 the city reached a total built-up area of 185 km^2, more than three times the former value (Fig. 2).

This rapid expansion goes hand in hand with a doubling of Dushanbe's population within the last 50 years, necessarily calling for a refinement of existing hazard and risk maps for Dushanbe and many other Central Asian capitals. The Earthquake Model Central Asia (EMCA; http://www.emca-gem.org, last accessed August 2013), a regional program of the Global Earthquake Model (GEM), aims at a cross-border assessment of seismic hazard and risk in Central Asia. Within this program, microzonation and vulnerability assessment activities are carried out in several large urban areas.

For the microzonation of Dushanbe (in contrast to previous studies [Zaslavsky, 1984, 1987] which only used pointwise estimates for a few sites in the city) we installed a dense temporary seismic network covering 72 sites. Moreover, noise recordings were collected by means of 37 single-station noise measurements as well as four micro-array configurations. Site effect studies are combined with first findings of previously realized vulnerability assessment based on satellite remote sensing and omnidirectional imaging. All measurements were taken in the actual administrative urban area of the town, as well as in the area to the west and to the south. In this study, we will describe the experiment and present our first results for identifying spatial ground-motion variability.

GEOLOGICAL AND GEOPHYSICAL SETTING

Situated at the confluence of two rivers, the Varzob and the Kafirnigan, present-day Dushanbe has around 650,000 inhabitants. The city is located in the central part of the Hissar valley, which is orientated east–west, limited to the north by the Hissar Range and to the south by the Babatag and Rangon ridges. In the territory of the city and its southern peripheral parts, Quaternary deposits are widespread. They tend to form accumulated terraces of ancient and modern valleys, also covering the lower parts of watersheds and slopes of ridges. These Quaternary sediments are interleaved by alluvial and diluvial sediments and their paragenetic combinations (Zodotarow

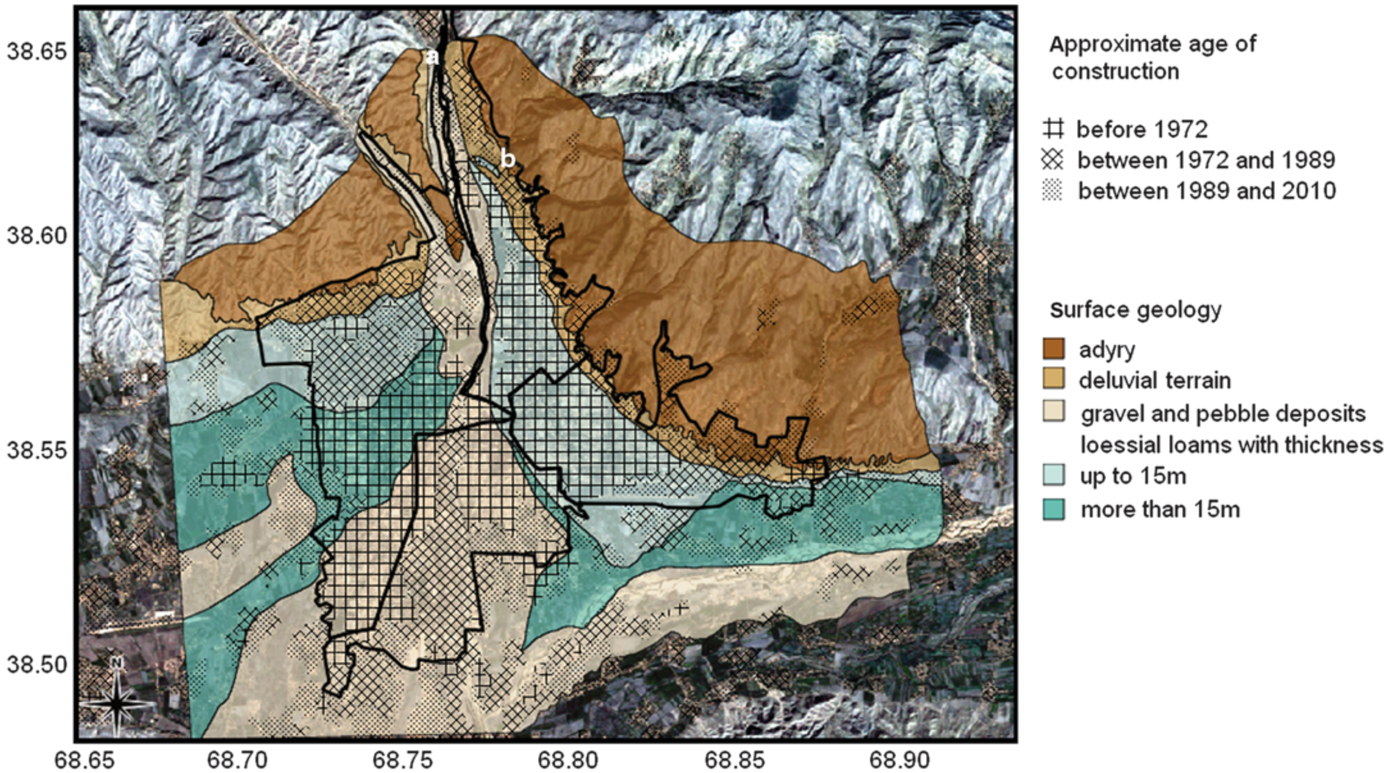

▲ **Figure 2.** Approximate age of built-up areas in Dushanbe derived from satellite images for three different time slices (1972, 1989, and 2010) covering the same spatial extent. Colors indicate surface soil materials (Zodotarow *et al.*, undated). Letters indicate the location of the photos shown in Figure 3. The thick black line represents today's administrative border of the city.

et al., undated). The thickness of the Quaternary deposits can be up to several hundred meters in the central part of the valley, but it decreases to a few meters at the foothills and in areas where the bedrock outcrops.

The territory east of the Varzob river (where 40% of building stock is located; see Fig. 2) differs also from the rest by the presence of thick macrospores loess-type soils (light greenish blue in Fig. 2) having high-subsidence features under watering. Of course, this fact negatively influences the technical conditions of buildings and structures. Therefore, some of the buildings and structures on the left-bank part of the city are observed to be deformed as a result of soil subsidence, therefore being highly vulnerable under seismic excitations (Jabarov and Yasunov, 2008). Moreover, nonlinear effects cannot be excluded; these have already been observed on the loess soils in the city during the 1989 **M** 5.5 Gissar earthquake (Babaev *et al.*, 2005). The homogeneous loess layers in the northwestern and northeastern districts of Dushanbe are expected to be particularly prone to nonlinear behavior during strong ground motion (Negmatulaev, Todorovska, Trifunac, 1999).

The central part of Dushanbe around the Varzob and Kafirnigan rivers is located on partially unconsolidated river terraces, which are covered with boulder and pebble deposits (light brown color in Fig. 2, photo (a) in Fig. 3). To the sides of the valley the clay content increases. In the northern periphery of the city, the basin boulder-pebble deposits are sometimes replaced by layers of poorly rounded boulders and limestone and sand-loam aggregates. The northeastern and northwestern foothills, which are called adyry in Tajikistan (brownish color in Fig. 2, photo (b) in Fig. 3), are covered by loess up to 15–20 m over dense clay, gravel layers, and sandstone.

TEMPORARY SEISMIC NETWORK INSTALLATION

Starting from 22 March 2012 a dense temporary seismic network was installed in Dushanbe (Fig. 4). The network consisted of 45 EDL 24-bit acquisition systems with the gain fixed to 1 equipped with short-period Mark-L4-C-3D sensors. This kind of sensor was found to be suitable for investigations down to 0.1 to 0.2 Hz (Strollo, Bindi, *et al.*, 2008; Strollo, Parolai, *et al.*, 2008). To increase the number of monitored sites in the inhabited area, 27 stations were relocated at the beginning of July 2012. For another 9 stations of the set of 45 stations, the sites were not changed and yet another 9 stations were removed completely (for station locations, see Ⓔ Table S1, available in the electronic supplement to this paper). All stations operated in continuous mode at a sampling rate of 100 samples per second until the removal of the entire network at the end of October 2012. However, due to problems with power supply at a few sites there are some gaps in the recordings. The exact recording times for all stations are listed in Ⓔ Table S1 (see electronic supplement).

The instruments were installed on the ground floor (or in cellars, if available) of private houses and public buildings with

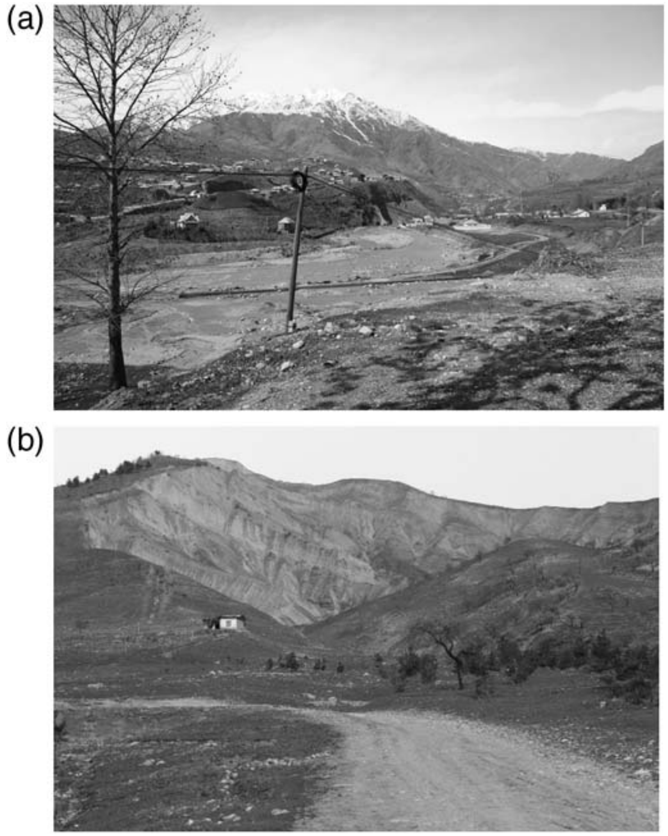

▲ **Figure 3.** (a) Unconsolidated boulder and pebble terraces of the Varzob river at the northern edge of the city. (b) Loess covering the foothills in the northeastern part of the city. Locations are indicated in Figure 2.

generally up to two floors, covering the entire urban area of Dushanbe. Two stations operating from March until October 2012 were installed outside the actual city with the aim of having a reference station for the site-effect estimation analysis. The station closer to the city could only be installed over a thin layer (some meters) of loess and gravel deposited on the slope of a hill. The other station Du01 was installed on outcropping Paleozoic rock (granite; Babaev and Liskov, 1974) around 20 km north of the city (therefore the site is not shown in Fig. 4).

From the continuous data streams of the network, the recordings of 292 earthquakes ($3.2 \leq \mathbf{M} \leq 7.2$) were extracted using a slightly modified version of the procedure proposed by Galiana-Merino *et al.* (2008). The distribution of the nearby epicenters is shown in Figure 1. The data set consists of 27 local and 257 regional events. We only included earthquakes with an epicentral distance to the network of at least five times the maximum interstation distance, to exclude any source and path effects for waves traveling to the stations. Finally, eight teleseismic events complete the data set. The different energy content of the earthquake recordings (due to different the hypocentral distances and magnitudes) allowed us to widen the investigated frequency range.

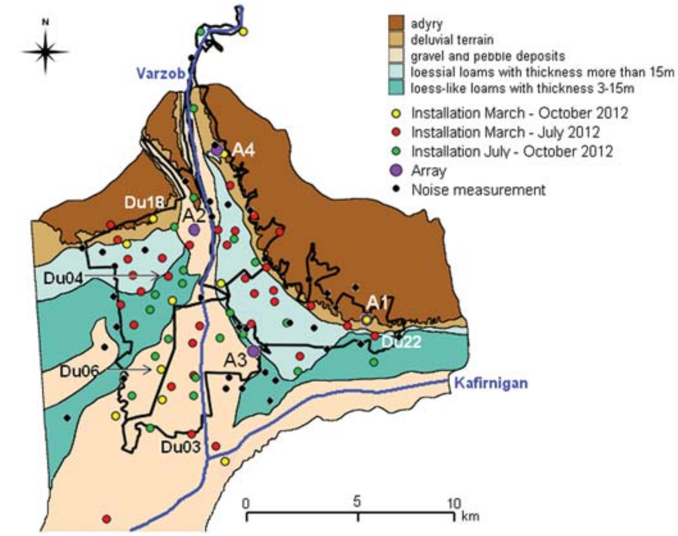

▲ **Figure 4.** Surface soils (Zodotarow *et al.*, undated). Colored dots, installation sites of the temporary seismic network; purple dots, array measurement sites; and black dots, noise measurement sites. Network installation sites and sites of array measurements mentioned in the text are labeled. The thick black lines are administrative borders of the city.

As an example, Figure 5 shows the detrended recordings at different sites in the city of an M_w 4.6 earthquake the epicenter of which was 150 km southeast of the city in the border region with Afghanistan. Because of the rather small aperture of the network at this distance clear differences between the waveforms mainly depend upon the location of the station and can hardly be explained by source effects. Not only does the amplitude ratio differ by more than a factor of two compared with reference station Du01, but there are also significant differences in the cumulative energy function due to longer shaking on soft soil sites. Remarkably, the cumulative energy for Du22 at the eastern edge of the city is ten times higher compared with the reference site Du01.

NOISE LEVEL IN THE CITY AND FREQUENCY RANGE OF INVESTIGATION

To investigate the appropriateness of the sensor–digitizer configuration and temporal (diurnal and seasonal) stability of the level of seismic noise at some characteristic sites, we processed the continuous time series by computing the probability density function (PDF) for a set of power spectral densities (PSDs), following McNamara and Buland (2004). We processed time series 900 s long, from which we removed the mean and the instrumental response. Each time series was divided into segments of 300 s, overlapping by 75 per cent, to reduce the variance in the PSD calculation (Cooley and Tukey, 1965). The total power, representing the PSD estimate, was obtained from the square of the amplitude spectrum multiplied by the standard normalization factor $2\Delta t/N$, in which Δt is the

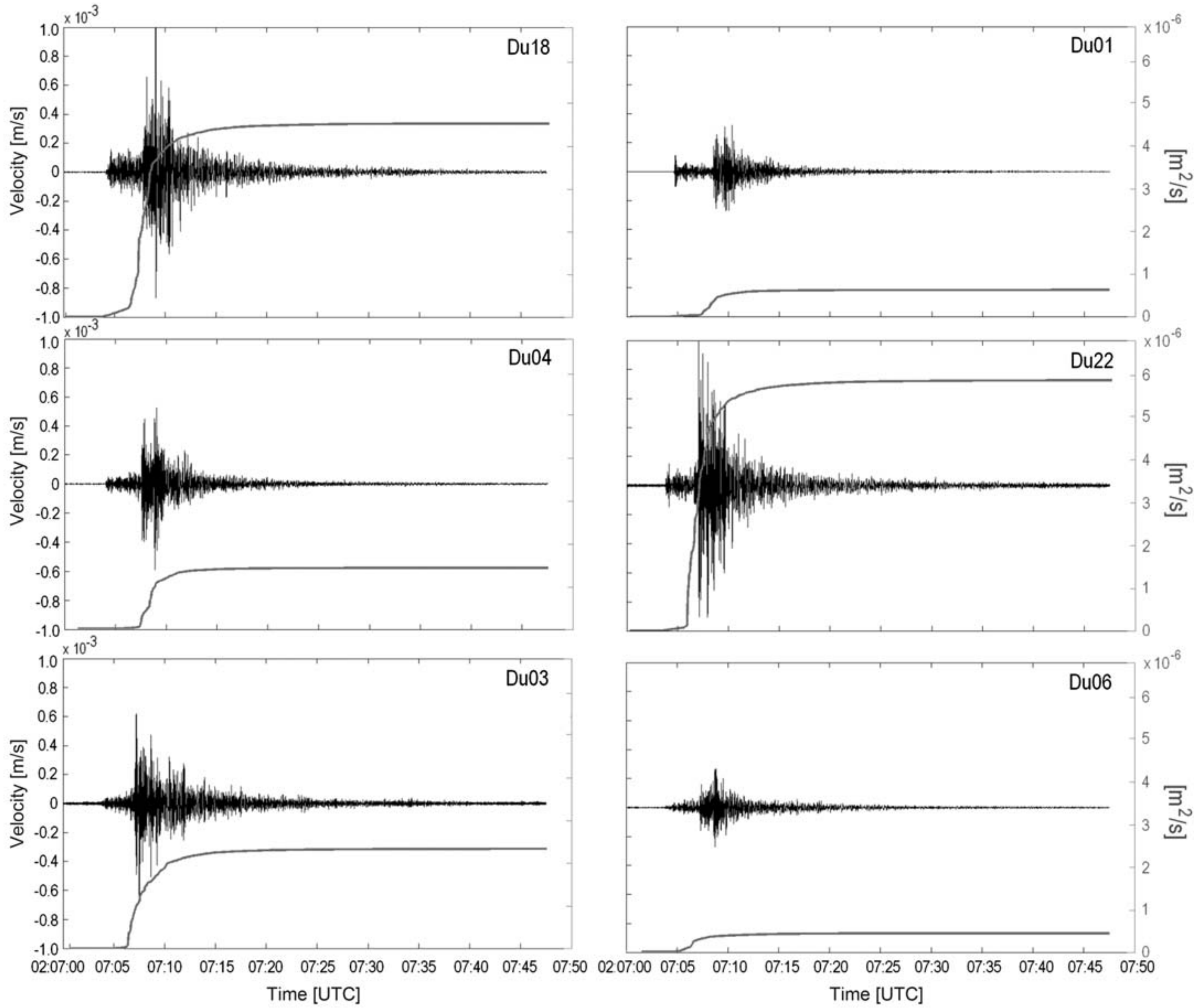

▲ **Figure 5.** Recordings at six different stations of the 29 June 2012 (M_w 4.6) earthquake. The panels are ordered corresponding to their geographic distribution. The gray line indicates the cumulative velocity square integral. In each panel, the station ID (Fig. 4) is shown.

sample interval and N is the number of samples (McNamara and Buland, 2004).

Figure 6 shows the PDFs computed for stations Du01 and Du03 over the period from 18 July until 25 October 2012. The PDFs of the reference station Du01, which was installed in a quiet area close to a small village, display rather stable noise conditions with very low power and only a 10 dB separation between the tenth and ninetieth percentiles in the high-frequency range, which represents relatively small diurnal variations of high-frequency cultural noise at this site. In the intermediate-frequency range between 0.8 and 3 Hz, a broad separation between the tenth and ninetieth percentiles can be found. Following Fyen (1990) and Burtin *et al.* (2008), this might be due to seismic noise caused by ground vibrations generated by bed-load transport of the Varzob river. This large river drains the Gissar mountain range north of Dushanbe and has a strongly variable water flow with its highest water level usually in June caused by glacier and snow melt (Vatanshoev, 2003). For very low frequencies, as expected, the self noise of the sensor exceeds the ambient noise level. Strollo, Parolai, *et al.* (2008) calculated theoretical self-noise power spectral densities (PSDs) for various sensor and acquisition system couples. Assuming for the sake of simplicity that the self noise starts to affect the PSD when the difference between the tenth percentile of the PDF distribution and the self-noise PSD becomes almost constant for decreasing frequencies, Figure 6 shows that the seismic-noise spectral levels can be retrieved for frequencies down to at least 0.2 Hz.

Correspondingly, also for station Du03, the PDF of the vertical component is reliable down to ~0.15 Hz. For low frequencies ($0.2 < f < 1$ Hz), the horizontal component PDFs are rather symmetric, with the highest probability being

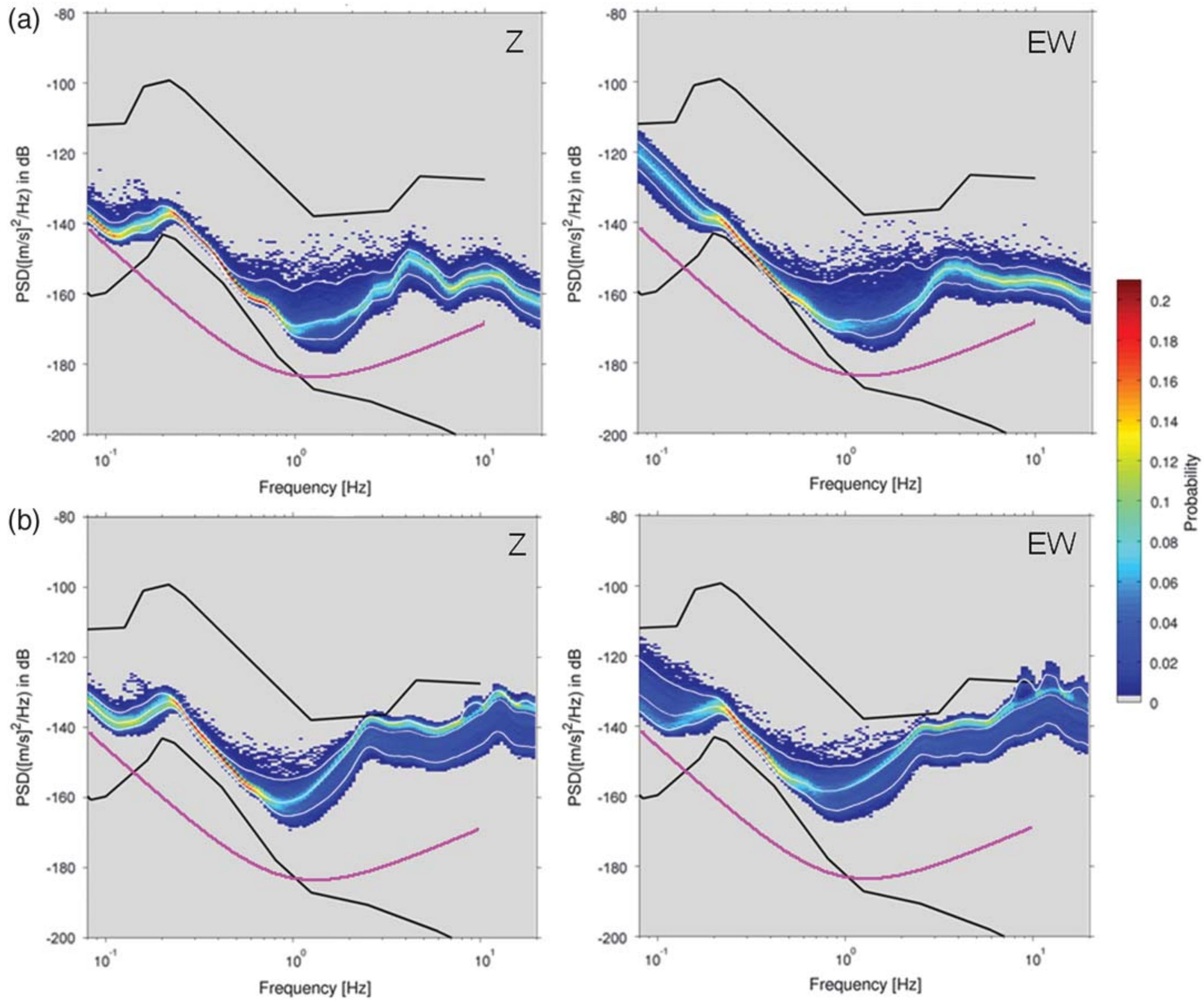

▲ **Figure 6.** Probability density function for the vertical and the east–west component for stations (a) Du01 and (b) Du03. The Peterson model (Peterson, 1993) is shown in black and the tenth, fiftieth, and ninetieth percentiles of the distribution are shown in white. The theoretical self-noise power spectral density (PSD) is represented by the pink curve.

found close to the fiftieth percentile. In contrast, at higher frequencies (> 1 Hz), the 20–30 dB separation between the tenth and ninetieth percentiles, notably significant for 8.5 and 12.5 Hz, reflects a significant diurnal variation in cultural noise due to human activity; this can easily be explained as Du03 was installed in an industrial area (e.g., McNamara and Buland, 2004). Therefore, although the stations in the city exhibit considerable variations in noise levels as a function of time of day, the detection of the amplification pattern is reliable down to 0.2 Hz.

SITE RESPONSE VARIATIONS ACROSS THE CITY

The spectral amplifications were computed by applying a reference site method, namely the standard spectral ratio technique (SSR; Borcherdt, 1970), through the comparison of earthquake recordings at the studied site with those of a reference station nearby. It is assumed that records from the reference site (in general, a station installed on outcropping of hard bedrock) contain the same source and propagation effects as records from the other sites. Therefore, the spectral ratio can directly provide the site response (Field and Jacob, 1995; Bonilla *et al.*, 1997; Parolai *et al.*, 2000; Frankel *et al.*, 2002).

Nonreference site techniques, such as the single horizontal-to-vertical (H/V) method, allow determining the site response by means of one single station only without making use of the recordings at a reference site close by. The H/V method is a combination of the receiver-function technique proposed by Langston (1979) and the method of Nakamura (1989), based on the approach of Nogoshi and Igarashi

(1970, 1971); it can, however, provide only a lower bound in terms of site amplification defined as the ratio of H/V motion at the surface, by assuming that the vertical component of ground motion is relatively uninfluenced by amplification effects during the propagation through the soil layers. Although Nakamura's approach was originally used for microtremors, it was later extended to earthquake recordings, initially being applied to earthquake *S* waves by Lermo and Chávez-Garcia (1993).

To investigate the site response for the reference site Du01 by means of the H/V method, we performed the analyses for a subset of events considering only frequencies with a signal-to-noise (SNR) ratio larger than 3 (estimated by considering the fast Fourier transform of a noise window as wide as the signal window). We corrected the recordings for the instrumental response. Spectral amplitudes were smoothed using the Konno and Ohmachi (1998) recording window ($b = 40$), ensuring the smoothing of numerical instabilities whereas preserving the major features of the earthquake spectra. The H/V spectral ratio for Du01 is shown in Figure 7.

As required for a reference station, the H/V spectral ratios for Du01 are almost flat, allowing us to calculate the SSRs for the remaining stations using the same subset of events and considering Du01 as a reference site. As shown in Figure 7, all other sites, being representative for the surrounding area, show a clear peak or even a broad frequency range of amplification. Stations Du04 and Du22, both located on loess deposits but on opposing edges of the city, show amplification in a range from $\sim$1 to $\sim$10 Hz. It has been demonstrated (Woolery and Street, 2002) that such broad H/V peaks can occur at sites with large near-surface shear-wave velocity contrasts and a complicated subsurface geometry. On the other hand, station Du03 shows a narrower peak, but its amplitudes are exceeding 4. As can be seen in Figures 2 and 4, many of the recently built houses at the southern edge of the city have been constructed in this area on the banks of the Varzob river, which are characterized by thick layers of gravel and pebble deposits, exposing these settlements to a high-hazard level.

It must be noted that there is a slight trough in the H/V of Du01 around 4 Hz due to a small de-amplification of horizontal ground motions due to concave topographic features (e.g., Chávez-García *et al.*, 1996; Yu and Haines, 2003). Correspondingly, this is causing peaks in the SSRs for the other sites at 4 Hz.

DISPERSION CURVES

In addition to the spectral amplification pattern, direct observations of local *S*-wave velocity–depth profiles are a key factor in seismic-hazard assessment and are widely used in engineering seismology. Examples include empirical predictions of strong ground motion (e.g., Boore *et al.*, 1997), site coefficients for building codes (BSSC, 2004) and the characterization of the liquefaction potential (e.g., Stokoe and Nazarian, 1985; Andrus and Stokoe, 2000). Ambient seismic noise is mainly composed of surface waves, and therefore contains vital information about the *S*-wave velocity structure, allowing dispersion curves to be obtained from array noise recordings (Zhang *et al.*, 1996).

Several approaches have been proposed in the literature by which to obtain information on the velocity of seismic-wave propagation in the low-velocity sedimentary cover from seismic noise recordings. In general, all methods for retrieving surface-wave dispersion curves are based on phase-coherency measurements between pairs (at least two) of signals. In the following, we made use of the extended spatial auto-correlation method (Ohori *et al.*, 2002; Okada, 2003), originally proposed by Aki (1957, 1965), as a statistical tool for the extraction of information from seismic noise. The method is based on the assumption that the seismic noise represents the sum of waves propagating without attenuation in a horizontal plane in different directions with different powers, but with the same phase velocity for a given frequency. Moreover, we assume that waves with different propagation directions and different frequencies are statistically independent. As outlined in Ohori *et al.* (2002), when these assumptions are verified, the space-correlation function for one single angular frequency ω_0, normalized to the power spectrum, can be expressed as a zero-order Bessel function depending only on ω_0, the phase velocity, and the interstation distance. Because experimental values of the azimuthally averaged spatial correlation function can be obtained from seismic noise measurements carried out by 2D seismic arrays with known interstation distances, by fitting these latter values to the theoretical Bessel function values, the phase velocity can be retrieved.

In March and October 2012, four arrays with seismic stations were installed in different parts of Dushanbe (see Fig. 4). Different array geometries were used with the selected range of interstation distances allowing for an optimal compromise between resolution at shallow depths and the maximum depth of investigation. Seismic noise was recorded at 100 Hz sampling rate for almost three hours. The Rayleigh-wave phase velocities were computed by analyzing the seismic noise recorded on the vertical component, using 240 windows of signal of 30 s length. In order to reduce leakage problems, each signal window was tapered for 5% of its length using a cosine function.

Both the calculated dispersion curves and the H/V spectral ratios were then used to estimate the corresponding local *S*-wave velocity profile, using a joint inversion scheme (Arai and Tokimatsu, 2005; Parolai *et al.*, 2005; Picozzi *et al.*, 2005), which allows the trade-off problem between the model parameters that hampers the separate inversion of these curves to be overcome. For the inversion we assumed that the soil structure varies only laterally. The validity of this assumption was investigated by computing the H/V curve for each station of the array using the recorded data, and checking their similarity (not shown). The resulting average H/V curve can be safely considered as being representative for the volume underneath the array. The inversion of dispersion and H/V curves was carried out fixing to 5 the number of layers overlying the half-space in the model. During the inversion procedure the thickness and the *S*-wave velocity for each layer could be varied

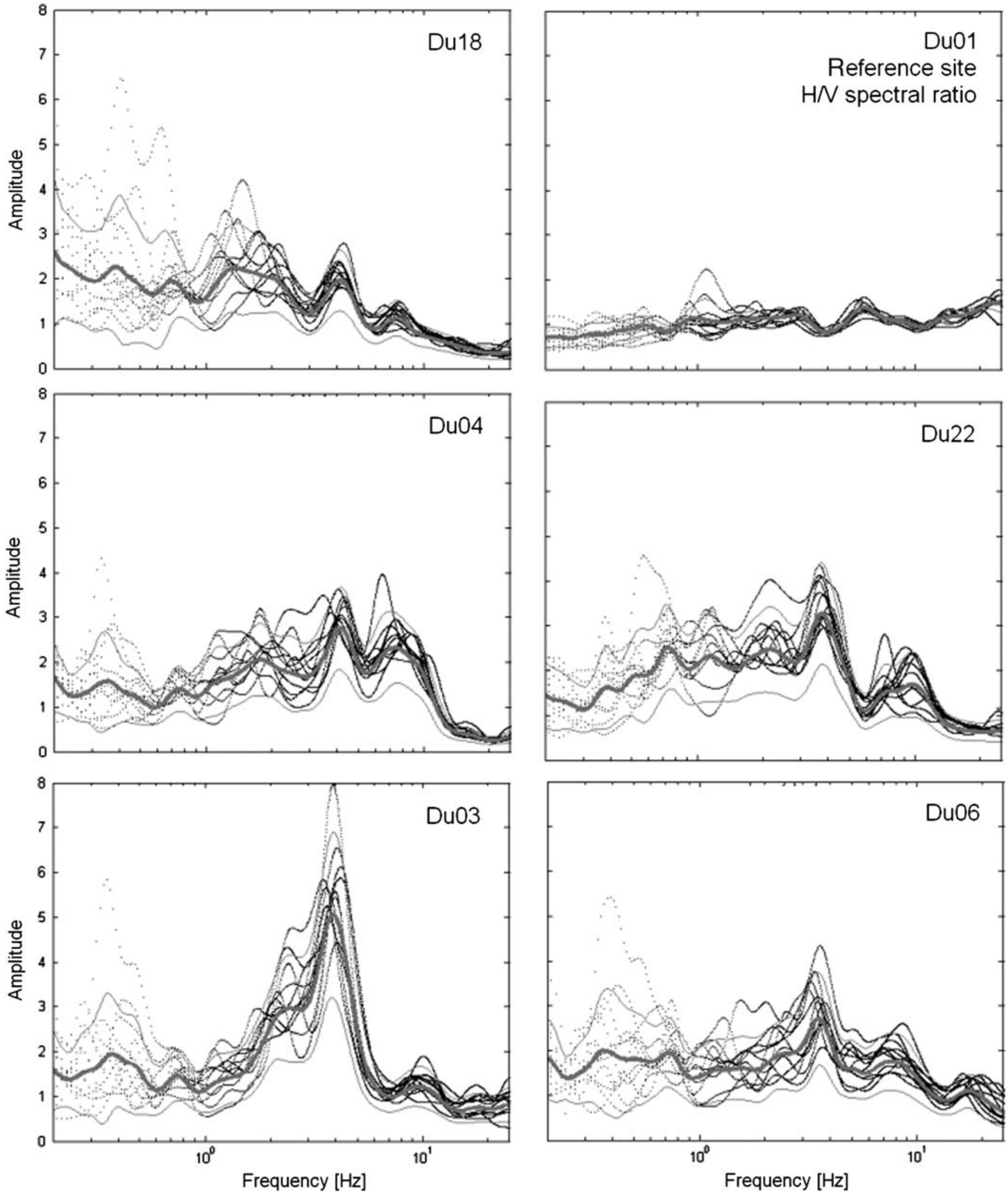

▲ **Figure 7.** Standard spectral ratios calculated for the *S*-wave window for the north–south component at each station and the corresponding spectrum at the station Du01. For Du01, the nearly flat response for the H/V spectral ratio is shown, indicating that Du01 is a suitable reference site. The black dots represent spectral ratios computed at frequencies for which the signal-to-noise ratio is greater than 3, whereas the gray curves represent the mean ratio±one standard deviation.

within predefined ranges. On the contrary, for each layer, *P*-wave velocity and density (values taken from Wang *et al.*, 2010), which have been shown to have much less influence on the inversion results, were assigned *a priori*.

The results of the inversion analysis for all array measurements are shown in Figure 8. Both the theoretical dispersion and H/V curves fit the observed values well. We note that for array A2 we performed the inversion using the dispersion curve alone, because the H/V curves for different sensors were perturbed by the presence of spurious, probably industrial, signals. It can be seen that the reliability of the inversion results is influenced not only by the quality of the input data, but also from the frequency range spanned by the H/V and dispersion curves. For A1 and A3 the dispersion and H/V curves occupy different frequency ranges (i.e., the fundamental resonance frequency is well below the frequencies of the dispersion curve). In these cases, they carry information for different depth ranges, with the dispersion curve mainly constraining the velocity in the surficial part of the model, and the H/V curve providing information about the *S*-wave velocity and impedance contrasts in the deeper part. However, being constrained by only the H/V curve, this part suffers more from trade-off between parameters, with the deeper part of the model being characterized by a higher uncertainty. This is also confirmed by the larger instability of the *S*-wave velocity profiles having misfits equal to best-fit +10%.

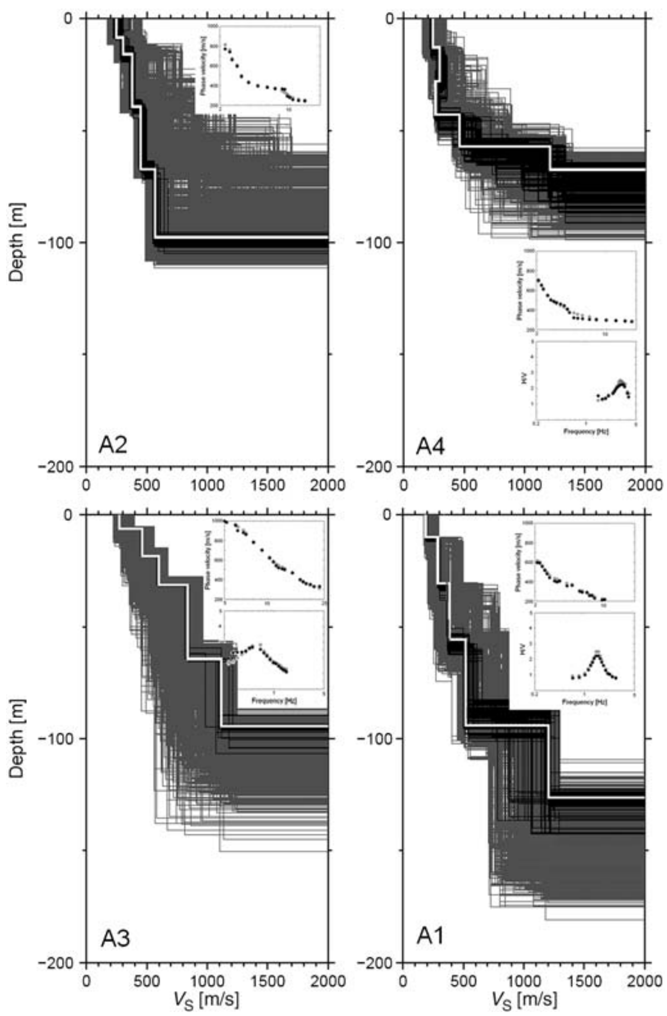

▲ **Figure 8.** Inversion results and fit to the dispersion and H/V ratio curves (insets) for four arrays. Thin gray lines, tested models; white line, the minimum cost model; and black lines, models lying inside the minimum cost +10% range. Top insets: Black dots, observed phase velocities and gray dots, the phase velocities for the minimum cost model. Bottom insets: black dots, average observed H/V ratio and white dots, the H/V ratio for the minimum cost model. The measurement sites are indicated in Figure 4.

The estimated *S*-wave velocity profiles provide a valuable overview of the different velocity structures and sediment cover thickness in the city. Array A3, located on gravel deposits overlain by a thin layer of loess, shows high *S*-wave velocities of almost 500 m/s below 10 m depth that increase up to more than 1000 m/s for the deepest parts. On the other hand, for A1 and A4, located on diluvial material, the *S*-wave velocities in the shallow layers are significantly lower (around 300 m/s down to 45 m for A4). As already observed in the past (Babaev *et al.*, 2005) these deep saturated low-velocity soil layers in the northwest of Dushanbe around array A4 seem to be particularly prone to nonlinear site amplification (Ni *et al.*, 1997; Hartzell *et al.*, 2004). For A1, also the deeper layers down to 100 m clearly show lower velocities. This goes in line with the findings in Figures 5 and 7, showing amplification and significant lengthening of ground shaking for site Du22. The thickness of the sedimentary cover varies from 65 m for A4 to 130 m for A1. In this context, the depth of the bedrock for arrays A1 and A3 is similar to published values found during groundwater studies nearby (Antonov and Gurshina, 1969).

VULNERABILITY ASSESSMENT BASED ON SATELLITE REMOTE SENSING AND OMNIDIRECTIONAL IMAGING

As outlined in the previous paragraphs, the complexity of seismic-geological conditions in combination with significant differences in the vulnerability of civil and industrial buildings calls for reliable assessment procedures for risk studies. In 2008, about 40% of the left-bank buildings in Dushanbe were analyzed for their vulnerability (Jabarov and Yasunov, 2008), concluding that several buildings and structures are in a deformed condition as the result of soil subsidence. In the period 2009/2010, a significant number of social infrastructure buildings were inspected visually and recommendations of preventive measures were made (P. Yasunov, personal comm., 2013).

However, as shown in Figure 2, the speed of the urban growth demands new methods for rapid and up-to-date assessment of earthquake vulnerability. To this end, the combination of satellite- and ground-based remote sensing methods allows for rapidly monitoring, classifying and regularly updating building inventories (Wieland *et al.*, 2012b). To this regard, an analysis of urban structures on the basis of medium-resolution satellite images can be performed on the district level. Using

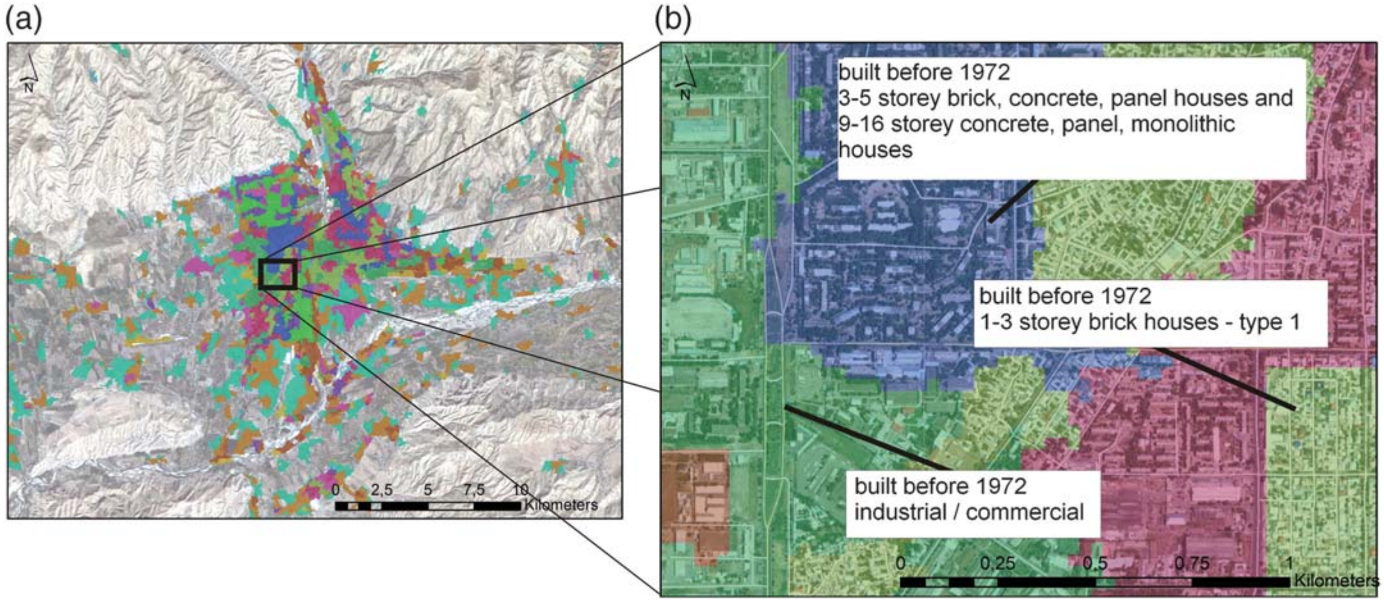

▲ **Figure 9.** Urban structure types represented by different colors showing areas of relatively homogeneous building types and construction age, derived from medium-resolution satellite image analysis for Dushanbe. (a) Zonation for the whole city of Dushanbe. (b) Close-up zonation, superimposed on a high-resolution satellite image for visualization.

image segmentation, multitemporal change detection and machine learning-based image classification, the urban environment can be delineated into areas of homogeneous urban-structure types, to provide a first estimate of the value and distribution of crucial vulnerability indicators, such as predominant building types, building ages, or urban-growth rates and distribution. Urban-structure types are in this study defined as spatial units at the block scale, which are homogeneous in medium-resolution satellite images in terms of their physical appearance (land cover) and usage (land use) as well as their approximate age (Wieland *et al.*, 2012a).

The delineation of the city into areas of homogeneous urban structure is shown in Figure 9. The urban structure types consist of 15 urban structure types (five building types in combination with three construction-age classes, which are shown in Fig. 2). The classification shows a clear dominance of 1–3 storey brick houses of different built-up density (greenish and turquoise colors in Fig. 9), which are mainly classified as highly vulnerable (A to B following the European Macroseismic Scale EMS-98 vulnerability classification). Remarkably, most of the newly built-up areas consist of this specific building type.

These results form the basis of a more detailed local assessment of the building stock using ground-based omnidirectional imaging. In summer 2012, all of the preselected sample areas were covered along a path of 176 km, recording a statistically significant number of buildings for each structure type. As shown in Pittore and Wieland (2012) for Bishkek, an analysis of such captured omnidirectional images can rapidly provide information on vulnerability-relevant features of buildings to be used for a first vulnerability classification.

CONCLUSIONS AND OUTLOOK

These preliminary findings already demonstrate that the complexity of the lithological succession, characterized by sharp lateral and vertical variations of the physical properties, will lead to significant variations of the amplification pattern and of the shear-wave velocity gradient over a short scale, emphasizing the need for an up-to-date site effect study for Dushanbe. To this regard, for the first time, a dense seismic network was installed in the city covering 72 sites, which will allow a better idea about differences in amplitude and lengthening of ground shaking with respect to a nearby rock site to be obtained. Moreover, data from 37 single-station noise measurements collected over an even denser grid will further allow the evaluation and the improvement of the spatial resolution of ground-motion variability, taking advantage of clustering and correlation analysis (Ullah *et al.*, 2012).

As the modification of strong ground shaking is strongly related to the *S*-wave velocity structure beneath the site, this parameter serves as a key factor in seismic-hazard assessment. The joint inversion of Rayleigh-wave dispersion and H/V curves allowed the retrieval of the *S*-wave velocity structure for four sites, at some sites down to more than one hundred meters. However, besides such point-wise estimates, large-scale site effect studies call for continuous seismic velocity models which can be obtained by correlation of seismic noise recordings. This method has gained considerable attention as a low-cost tool (Picozzi *et al.*, 2009; De Siena *et al.*, 2010; Pilz *et al.*, 2012) and will also be carried out for the urban area of Dushanbe.

In combination with already existing regional seismic intensity studies (Bindi *et al.*, 2011, 2013), which did not allow a conclusion to be drawn about the existence of any possible regional dependency in the intensity-attenuation characteristics, such highly detailed site information is crucial when assessing seismic risk, which is defined as the probability of occurrence of economic and social losses as a consequence of an earthquake. As shown by Figure 2, this is particularly important for the city of Dushanbe, the political and economic center of Tajikistan, which is experiencing steady demographic growth. This leads to an un-resisted growth of informal settlements and urban sprawling. To launch risk-mitigation strategies, a combination of detailed site-response information with new satellite- and ground-based remote sensing methods can be used for compiling a multiparameter database of inventory features as well as for the rapid monitoring and regularly updating of the building stock, and thus the local earthquake vulnerability. Therefore, in the field of earthquake risk reduction, an interdisciplinary exchange of expert knowledge from both civil engineering and remote sensing, as well as an integrated combination of methods, is a vital solution.

In the end, a reliable evaluation of the seismic risk on a local scale, together with a realistic assessment of the assets that are exposed to seismic hazard and their structural vulnerability, can, in the future, be used to undertake proper mitigation actions and to promptly and efficiently react to a potential catastrophic event. When the findings of the site effects are available, they will be combined with an updated zonation of building vulnerability. Moreover, further studies are being planned in which the behavior of characteristic building typologies in the city of Dushanbe will be monitored through the indoor installation of seismic sensors on different levels of selected buildings. Altogether, this enlarged data set will provide an even more detailed picture in terms of seismic hazard, vulnerability, and risk for the city of Dushanbe.

ACKNOWLEDGMENTS

We would like to acknowledge the Editor J. Lees and two anonymous reviewers for providing helpful comments that allowed us to significantly improve the manuscript. We are also very grateful for the collaboration and support given to us during the survey measurements and the data collection by many people in Dushanbe. We thank Erwin Guenther (GFZ), Asad Abdulkodirov, Shuhrat Pallaev, Faridun Khudonazarov (FOCUS Tajikistan), Faheem Merchant, Firuz Davlatyorov (Disaster Risk Management Initiative) as well as the technical staff of the Institute of Geology, Earthquake Engineering and Seismology of the Academy of Sciences of the Republic of Tajikistan for their help during the field work. Kevin Fleming and Abdallah Jamal kindly revised our English. Instruments were provided by the Geophysical Instrumental Pool Potsdam (GIPP) and by the Central Asian Institute for Applied Geosciences (CAIAG). This research has been supported by the Global Change Observatory Central Asia of the GFZ, the Earthquake Model Central Asia (EMCA), the European Commission's Department of Humanitarian Aid and Civil Protection (ECHO) under DIPECHO VII and the Aga Khan Development Network.

REFERENCES

Aki, K. (1957). Space and time spectra of stationary stochastic waves, with special reference to microtremors, *Bull. Earthq. Res. Inst. Tokyo Univ.* **35,** 415–456.

Aki, K. (1965). A note on the use of microseisms in determining the shallow structures of the earth's crust, *Geophysics* **29,** 665–666.

Andrus, R. D., and K. H. Stokoe (2000). Liquefaction resistance of soils from shear-wave velocity, *J. Geotech. Geoenviron. Eng. ASCE* **126,** 1015–1025.

Antonov, J. K., and N. M. Gurshina (1969). On the state of exploitation and protection of underground water in the area of the Tajik SSR, *Rep. Acad. Sci. Tajik SSR* **12,** 53 pp. (in Russian).

Arai, H., and K. Tokimatsu (2005). *S*-wave velocity profiling by joint inversion of microtremor dispersion curve and horizontal-to-vertical (H/V) spectrum, *Bull. Seismol. Soc. Am.* **95,** 1766–1778.

Babaev, A. M., and A. M. Liskov (1974). Main features of the geological structures of the Dushanbe test field region, in *The Search for Earthquake Forerunners at Prediction Test Fields*, Nauka, Moscow, 41–48 (in Russian).

Babaev, A. M., A. R. Ischuk, and S. K. Negmatulaev (2005). *Seismic Conditions of the Territory of Tajikistan*, Publication of the International University of Tajikistan, Dushanbe, 93 pp.

Bindi, D., A. A. Gomez Capera, S. Parolai, K. Abdrakhmatov, M. Stucchi, and J. Zschau (2013). Location and magnitudes of earthquakes in Central Asia from seismic intensity data: Model calibration and validation, *Geophys. J. Int.* **192,** 710–724.

Bindi, D., S. Parolai, A. Oth, K. Abdrakhmatov, A. Muraliev, and J. Zschau (2011). Intensity prediction equations for Central Asia, *Geophys. J. Int.* **187,** 327–337.

Bonilla, L. F., J. H. Steidl, G. T. Lindley, A. G. Tumarkin, and R. J. Archuleta (1997). Site amplification in the San Fernando valley, California: Variability of site effect estimation using *S*-wave, coda, and *H*/*V* methods, *Bull. Seismol. Soc. Am.* **87,** 710–730.

Boore, D. M., W. B. Joyner, and T. E. Fumal (1997). Equations for estimating horizontal response spectra and peak acceleration from western North American earthquakes: A summary of recent work, *Seismol. Res. Lett.* **68,** 128–153.

Borcherdt, R. D. (1970). Effects of local geology on ground motion near San Francisco Bay, *Bull. Seismol. Soc. Am.* **60,** 29–61.

Building Seismic Safety Council (BSSC) (2004). *NEHRP Recommended Provisions for Seismic Regulations for New Buildings and Other Structures*, 2003 edition (FEMA 450), Building Seismic Safety Council, National Institute of Building Sciences, Washington, D.C., USA, 353 pp.

Bune, V. I., and G. P. Gorshkov (1980). *Seismic Zonation of USSR*, Nauka, Moscow, 307 pp. (in Russian).

Burtin, A., L. Bollinger, J. Vergne, R. Cattin, and J. L. Nabelek (2008). Spectral analysis of seismic noise induced by rivers: A new tool to monitor spatiotemporal changes in stream hydrodynamics, *J. Geophys. Res.* **113,** B05301, doi: 10.1029/2007JB005034.

Burtman, V. S., and P. Molnar (1993). Geological and geophysical evidence for deep subduction of continental crust beneath the Pamir, *Spec. Pap. Geol. Soc. Am.* **281,** 1–76.

Chávez-García, F. J., L. R. Sánchez, and D. Hatzfeld (1996). Topographic site effects and HVSR. A comparison between observations and theory, *Bull. Seismol. Soc. Am.* **86,** 1559–1573.

Cohen, L. A., J. M. Mirzobaev, G. O. Oripov, and A. Romanov (1975). *Map of the Seismic Zonation of Dushanbe*, Soviet Academy of Science, Moscow (scale 1:25,000) (in Russian).

Cooley, J. W., and J. W. Tukey (1965). An algorithm for machine calculation of complex Fourier series, *Math. Comput.* **19,** 297–301.

Delvaux, D., S. Cloetingh, F. Beekman, D. Sokoutis, E. Burov, M. M. Buslov, and K. E. Abdrakhmatov (2013). Basin evolution in a folding lithosphere: Altai–Sayan and Tien Shan belts in Central Asia, *Tectonophysics* **602,** 194–222, doi: 10.1016.j.tecto.2013.01.010.

De Siena, L., E. Del Pezzo, and F. Bianco (2010). Seismic attenuation imaging of Campi Flegrei: Evidence of gas reservoirs, hydrothermal basins, and feeding systems, *J. Geophys. Res.* **115,** B09312, doi: 10.1029/2009JB006938.

Fan, G., J. Ni, and T. Wallace (1994). Active tectonics of the Pamir and Karakorum, *J. Geophys. Res.* **99,** 7131–7160.

Field, E. H., and K. H. Jacob (1995). A comparison and test of various site response estimation techniques, including three that are non reference-site dependent, *Bull. Seismol. Soc. Am.* **86,** 991–1005.

Frankel, A. D., D. L. Carver, and R. A. Williams (2002). Nonlinear and linear site response and basin effects in Seattle for the $M = 6.8$ Nisqually, Washington, earthquake, *Bull. Seismol. Soc. Am.* **92,** 2090–2109.

Fyen, J. (1990). Diurnal and seasonal variations in the microseismic noise level observed at the NORESS array, *Phys. Earth Planet. In.* **63,** 252–268.

Galiana-Merino, J. J., J. L. Rosa-Herranz, and S. Parolai (2008). Seismic P phase picking using a kurtosis-based criterion in the stationary wavelet domain, *IEEE Trans. Geosci. Remote Sensing* **46,** 3815–3826, doi: 10.1109/TGRS.2008.2002647.

Giardini, D. (1999). The global seismic hazard assessment program (GSHAP)—1992/1999, *Ann. Geofisc.* **42,** 957–974.

Gubin, I. (1960). *Patterns of Seismic Events in the Territory of Tajikistan*, Soviet Academy of Science, Moscow, 464 pp. (in Russian).

Hartzell, S., L. F. Bonilla, and R. A. Williams (2004). Prediction of nonlinear soil effects, *Bull. Seismol. Soc. Am.* **94,** 1609–1629.

Jabarov, M. D., and P. Yasunov (2008). Inventory and survey of multi-storey dwelling buildings in a left-bank part of Dushanbe city, in *Strengthened Disaster Risk Management (DRM) in Tajikistan*, United Nations Development Program–Disaster Risk Management Project (UNDP–DRMP) report, New York, U.S.A., 1–26.

Katok, A. P. (1965), The Khait earthquake of 1949 July 10: Effect on regime of Dushanbe/Garm, USSR, *DANTA* **8,** 14 (in Russian).

Khalturin, V., L. Dwelley, and B. Tucker (1997). *Lessons for Central Asia from Armenia to Sakhalin: Strategies for Urban Earthquake Risk Management for the Central Asian Republics*, GeoHazards Int., Vol. 10, Stanford, California, U.S.A.

Konno, K., and T. Ohmachi (1998). Ground-motion characteristics estimated from spectral ratio between horizontal and vertical components of microtremor, *Bull. Seismol. Soc. Am.* **88,** 228–241.

Langston, C. A. (1979). Structure under Mount Rainier, Washington inferred from teleseismic P waves, *Geophys. Res. Lett.* **84,** 4749–4762.

Lermo, J., and F. J. Chávez-Garcia (1993). Site effect evaluation using spectral ratios with only one station, *Bull. Seismol. Soc. Am.* **83,** 1574–1594.

McNamara, D. E., and R. P. Buland (2004). Ambient noise levels in the continental United States, *Bull. Seismol. Soc. Am.* **94,** 1517–1527.

Medvedev, S. V. (1952). Evaluation of seismic intensity as a function of ground conditions, *Geol. Inst. Soviet Acad. Sci.* **14,** 29–52.

Molnar, P., and P. Tapponnier (1975). Cenozoic tectonics of Asia: Effects of a continental collision, *Science* **189,** 419–426.

Nakamura, Y. (1989). A method for dynamic characteristics estimations of subsurface using microtremors on the ground surface, *Q. Rep. Railway Tech. Res. Inst. Japan* **30,** 25–33.

Nazarov, A. G., and B. A. Nechaev (1953). *Seismic Microzonation Map: The Administrative Area of Stalinabad*, Soviet Academy of Science, Moscow, Russia (in Russian).

Negmatulaev, S., A. Ischuk, and Y. Potekhin (1999). Seismic hazard and building vulnerability in Tajikistan, *NATO Asi Series* **52,** 107–125.

Negmatulaev, S. K., M. I. Todorovska, and M. D. Trifunac (1999). Simulation of strong earthquake motion by explosions—Experiments at the Lyaur testing range in Tajikistan, *Soil Dynam. Earthq. Eng.* **18,** 189–207.

Ni, S. D., R. V. Siddharthan, and J. G. Anderson (1997). Characteristics of nonlinear response of deep saturated soil deposits, *Bull. Seismol. Soc. Am.* **87,** 342–355.

Nogoshi, M., and T. Igarashi (1970). On the propagation characteristics of microtremors, *J. Seismol. Soc. Japan* **23,** 264–280 (in Japanese with English abstract).

Nogoshi, M., and T. Igarashi (1971). On the amplitude characteristics of microtremor, *J. Seismol. Soc. Japan* **24,** 26–40 (in Japanese with English abstract).

Nurmangambetov, A., N. Mikhailova, and W. Iwan (1999). Seismic hazard of the Central Asian region, in *Seismic Hazard and Building Vulnerability in Post-Soviet Central Asian Republics*, S. A. King, V. I. Khalturin, and B. E. Tucker (Editors), Kluwer Academic Publishers, Nederlands, 1–43.

Ohori, M., A. Nobata, and K. Wakamatsu (2002). A comparison of ESAC and FK methods of estimating phase velocity using arbitrarily shaped microtremor arrays, *Bull. Seismol. Soc. Am.* **92,** 2323–2332.

Okada, H. (2003). The microtremor survey method, *American Geophysical Monograph* 12, American Geophysical Union, Washington, D.C., 1–14.

Parolai, S., D. Bindi, and P. Augliera (2000). Application of the generalized inversion technique (GIT) to a microzonation study: Numerical simulations and comparison with different site-estimation techniques, *Bull. Seismol. Soc. Am.* **90,** 286–297.

Parolai, S., M. Picozzi, S. Richwalski, and C. Milkereit (2005). Joint inversion of phase velocity dispersion and H/V ratio curves from seismic noise recordings using a genetic algorithm, considering higher modes, *Geophys. Res. Lett.* **32,** L01303, doi: 10.1029/2004GL021115.

Peterson, J. (1993). Observations and modeling of seismic background noise, *U.S. Geol. Surv. Open-File Rept. 93-322*, Albuquerque, New Mexico, U.S.A., 93–95.

Picozzi, M., S. Parolai, and S. Richwalski (2005). Joint inversion of H/V ratios and dispersion curves from seismic noise: Estimating the S-wave velocity of bedrock, *Geophys. Res. Lett.* **32,** L11308.

Picozzi, M., S. Parolai, D. Bindi, and A. Strollo (2009). Characterization of shallow geology by high-frequency seismic noise tomography, *Geophys. J. Int.* **176,** 164–174.

Pilz, M., S. Parolai, M. Picozzi, and D. Bindi (2012), Three-dimensional shear wave velocity imaging by ambient seismic noise tomography, *Geophys. J. Int.* **189,** 501–512.

Pittore, M., and M. Wieland (2012), Toward a rapid probabilistic seismic vulnerability assessment using satellite and ground-based remote sensing, *Nat. Hazards* **16,** no. 1, 115–145, doi: 10.1007/s11069-012-0475-z.

Pomonis, A. (1990), The Spitak (Armenia, USSR) earthquake: Residential building typology and seismic behavior, *Disasters* **14,** 89–114.

Rautian, T., and W. Leith (2002). Composite regional catalogs of earthquakes from the former Soviet Union, *U.S. Geol. Surv. Open-File Rept. 02-500*, 53 pp.

Stokoe, K. H., and S. Nazarian (1985). Use of Rayleigh waves in liquefaction studies, in *Measurement and Use of Shear Wave Velocity for Evaluating Dynamic Soil Properties*, R. D. Woods (Editor), ASCE, New York, U.S.A., 1–17.

Strollo, A., D. Bindi, S. Parolai, and K. H. Jäckel (2008). On the suitability of 1 s geophone for ambient noise measurements in the 0.1–20 Hz frequency range: Experimental outcomes, *Bull. Earthq. Eng.* **6,** 141–147.

Strollo, A., S. Parolai, K. H. Jäckel, S. Marzorati, and D. Bindi (2008). Suitability of short-period sensors for retreiving reliable H/V peaks for frequencies less than 1 Hz, *Bull. Seismol. Soc. Am.* **98,** 671–681.

Trifonov, V. G., O. V. Soboleva, R. V. Trifonov, and G. A. Vostrikov (2002). Recent geodynamics of the Alpine-Himalayan collision belt, *Trans Geol. Inst. RAS* **541,** 224 pp. (in Russian).

Tsshoher, V. O. (1938). *Seismic Zonation of the Urban Area and Antiseismic Engineering Building Codes*, Soviet Academy of Science, Moscow, Russia, 103 pp. (in Russian).

Ullah, S., D. Bindi, M. Pittore, M. Pilz, S. Orunbaev, B. Moldobekov, and S. Parolai (2012). Improving the spatial resolution of ground motion variability using earthquake and seismic noise data: The example of Bishkek (Kyzrgyzstan), *Bull. Earthq. Eng.* **11,** no. 2, 385–399, doi: 10.1007/s10518-012-9401-8.

Vatanshoev, V. (2003). Rivers and lakes of Tajikistan. Hydrometerological Observations of the Nature, Ministry of Nature Protection of the Republic of Tajikistan (Editor), Dushanbe, Tajikistan, 23 pp. (in Russian).

Wang, X. T., T. G. Berhe, S. Webb, and W. Wu (2010). Dynamic stability analysis of landfill slope in Dushanbe, Tajikistan, in *Advances in Environmental Geotechnics*, Y. Chen, X. Tang, and L. Zhan (Editors), Springer, Berlin, Germany, 420–425.

Wieland, M., M. Pittore, S. Parolai, and J. Zschau (2012a). Exposure estimation from multi-resolution optical satellite imagery for seismic risk assessment, *ISPRS Int. J. Geo-Inf.* **1,** 69–88.

Wieland, M., M. Pittore, S. Parolai, J. Zschau, B. Moldobekov, and U. Begaliev (2012b). Estimating building inventory for rapid seismic vulnerability assessment: Towards an integrated approach based on multi-source imaging, *Soil Dyn. Earthq. Eng.* **36,** 70–83.

Woolery, E. W., and R. Street (2002). 3D near-surface soil response from H/V ambient noise ratios, *Soil Dynam. Earthq. Eng.* **22,** 865–876.

Yu, J., and J. Haines (2003). The choice of references sites for seismic ground amplification analyses: Case study at Parkway, New Zealand, *Bull. Seismol. Soc. Am.* **93,** 713–723.

Zaslavsky, Y. (1984). High frequency noise spectra at the Dushanbe seismological observatory, in *Earthquakes of Central Asia and Kazakhstan*, United Services for Earthquake Research (ESSN), Moscow, USSR, 175–184 (in Russian).

Zaslavsky, Y. (1987). *Analysis of Microseisms at the Dushanbe Seismological Observatory, Instruments and Methods of Earthquake Registration*, Nauka, Moscow, Russia, 152–157 (in Russian).

Zhang, B., M. Yu, C. Q. Lan, and W. Xiong (1996). Elastic waves and excitation mechanism of surface waves in multilayered media, *J. Acoust. Soc. Am.* **100,** 3527–3538.

Zodotarow, G. S., W. S. Fachorenko, W. I. Lipmija, D. Hergow, N. A. Rohdijow, and P. Jaodokowa (undated). *Polygon-Based Engineering and Geological Map of the Dushanbe Region*, Soviet Academy of Science, Moscow, Russia (in Russian).

Marco Pilz
Dino Bindi
Tobias Boxberger
Massimiliano Pittore
Jacek Stankiewicz
Shahid Ullah
Marc Wieland
Stefano Parolai
Helmholtz Center Potsdam
German Research Center for Geosciences
Helmholtzstr. 7
14467 Potsdam, Germany
pilz@gfz-potsdam.de

Farhod Hakimov
Shohrukh Murodkulov
Pulat Yasunov
Institute of Geology, Earthquake Engineering and Seismology
Academy of Sciences of the Republic of Tajikistan
Ayni Street 267
734063 Dushanbe, Tajikistan

Bolot Moldobekov
Sagynbek Orunbaev
Central Asian Institute for Applied Geosciences
Timur Frunze Street 73/2
720027 Bishkek, Kyrgyzstan

Firoz Verjee
Aga Khan Development Network
Disaster Risk Management Initiative
Ayni Street 24a
730025 Dushanbe, Tajikistan